Appl. Math. Mech. -Engl. Ed., **41**(10), 1497–1516 (2020)

APPLIED MATHEMATICS AND MECHANICS (ENGLISH EDITION)

https://doi.org/10.1007/s10483-020-2670-6

Bending and free vibrational analysis of bi-directional functionally graded beams with circular cross-section*

Yong HUANG†

School of Mathematics and Big Data, Foshan University,
Foshan 528000, Guangdong Province, China

(Received Mar. 30, 2020 / Revised Jul. 27, 2020)

Abstract The bending and free vibrational behaviors of functionally graded (FG) cylindrical beams with radially and axially varying material inhomogeneities are investigated. Based on a high-order cylindrical beam model, where the shear deformation and rotary inertia are both considered, the two coupled governing differential motion equations for the deflection and rotation are established. The analytical bending solutions for various boundary conditions are derived. In the vibrational analysis of FG cylindrical beams, the two governing equations are firstly changed to a single equation by means of an auxiliary function, and then the vibration mode is expanded into shifted Chebyshev polynomials. Numerical examples are given to investigate the effects of the material gradient indices on the deflections, the stress distributions, and the eigenfrequencies of the cylindrical beams, respectively. By comparing the obtained numerical results with those obtained by the three-dimensional (3D) elasticity theory and the Timoshenko beam theory, the effectiveness of the present approach is verified.

Key words higher-order beam theory, circular cross-section, bi-directional functionally graded (FG) beam, bending analysis, free vibration

Chinese Library Classification O321
2010 Mathematics Subject Classification 70J10, 74K10, 74H45

1 Introduction

Compared with traditional laminated materials, functionally graded (FG) materials can significantly reduce the risk for delamination failures. As a result, many kinds of structures fabricated by FG materials, including beams, plates, and shells, have been used in many different fields of engineering, and have been widely studied by various theories[1–10].

If a Timoshenko or higher-order beam model is adopted to investigate the free vibrations of axially FG beams, two coupled governing differential equations with variable coefficients will be derived, which makes it difficult to obtain the exact solutions due to the arbitrary gradient changes. Many researchers have introduced different numerical methods to solve such

* Citation: HUANG, Y. Bending and free vibrational analysis of bi-directional functionally graded beams with circular cross-section. *Applied Mathematics and Mechanics* (*English Edition*), **41**(10), 1497–1516 (2020) https://doi.org/10.1007/s10483-020-2670-6

† Corresponding author, E-mail: hyhy1223@hotmail.com

Project supported by the Natural Science Foundation of Guangdong Province of China (No. 2018A030313258)

problems. Based on the finite element method, Shahba et al.[11] discussed the free vibrations of arbitrarily tapered and axially FG Timoshenko beams under various boundary conditions. Huang et al.[12] introduced a unified method to analyze the free vibrations of Timoshenko beams with arbitrarily axial material parameters by transforming the governing equations into a system of linear algebraic equations under different boundary conditions. Based on the differential transformation element method, Rajasekaran and Tochaei[13] studied the free vibrations of axially FG Timoshenko beams. Tang et al.[14] studied the free vibrations of non-uniform FG Timoshenko beams, and derived the frequency equations in closed form, where the material properties were assumed to vary in a unified exponential law. Cao et al.[15] used the asymptotic development method to discuss the vibrational behaviors of uniform axially FG beams under different boundary conditions. Zhang et al.[16] presented an effective approximation to investigate the free vibrations of axially FG beams based on the Euler beam theory and the Timoshenko beam theory, respectively.

FG beams with bi-directional variations of material parameters have attracted increasing attention by many scholars recently[17–18] since bidirectional FG structures have better mechanical properties and can produce more effective resistance effects and realize the integrated design of materials and structures. With the symplectic method and the Hamiltonian state space approach, Zhao et al.[19] derived the elasticity bending solutions of the bi-directional FG beams under arbitrary lateral loadings. Based on the classical hairbrush hypothesis, Pydah and Sabale[20] obtained an analytical solution for the flexure of bi-directional FG circular beams subject to various tip loads. Armagan[21] presented a symmetric smoothed particle hydrodynamics method to derive the bending solutions of bi-directional FG beams under various boundary conditions with the Euler-Bernoulli, Timoshenko, and Reddy-Bickford beam theories, respectively. Li et al.[22] proposed a meshless total Lagrangian corrective smoothed particle method to study the static behavior of bi-directional FG beams with the exponential or power-law gradient assumption. Based on the Euler-Bernoulli and Timoshenko beam theories, Simsek[23] used the energy approach to analyze the free and forced vibrations of bi-directional FG beams subject to the action of moving loads. With the assumption of an exponential-law material distribution, Deng and Chen[24] introduced the variable substitution method and the dynamic stiffness matrix method to discuss the dynamic characteristics of bi-directional FG Timoshenko beams. Huynh et al.[25] used the isogeometric analysis method to study the free vibrations of bi-directional FG Timoshenko beams with power- and exponential-law models of material distributions, respectively. Nguyen et al.[26] introduced a finite element method to discuss the vibrations of bi-directional FG Timoshenko beams under the action of a moving concentrated loading. Based on the third-order shear deformation theory, Karamanli[27] investigated the free vibrations of bi-directional FG beams with exponentially graded material properties. Lal and Dangi[28] used the first-order shear deformation theory and Eringen's nonlocal elasticity theory to study the vibrational behavior of bi-directional FG non-uniform Timoshenko nanobeams, where the material properties varied in both the axial and the thickness directions according to the power- and exponential-law distributions, respectively.

It should be noted that most of the above mentioned papers are limited to FG beams with a rectangular cross-section. However, there are very few bending and eigenfrequency results reported for FG circular cylinders with radially or/and axially varying material inhomogeneities. Abadikhah and Folkow[29] adopted the three-dimensional (3D) elastodynamic theory to study the dynamic behaviors of simply supported FG cylinders with power- and exponential-law distributions of the material properties. Zhang et al.[30] introduced a higher-order shear deformation based spectral element model to calculate the stochastic natural frequency of radially FG beams with a circular cross-section. To the author's best knowledge, the bending and free vibrations of axially or two-dimensional (2D) FG cylindrical beams have not yet been reported. Solid circular beams are common structural elements in macro and micro scales. The analysis on the bending and free vibrations of FG cylindrical beams is useful for the precise design of

circular cylindrical composite beams.

The purpose of this paper is to introduce a high-order circular beam model for studying the bending and free vibrations of 2D FG circular beams, where the shear-free surface condition is identically satisfied. The analytical bending solutions can be obtained for general cases with different boundary conditions. By use of a new auxiliary function, a single governing equation is furthermore derived in the free vibration analysis of 2D FG circular beams. The Chebyshev polynomials are used to get the characteristic equations. Illustrative examples are given to show the effects of the gradient parameters on the deflections, the stresses, and the natural frequencies, respectively.

2 Theory and formulation

An elastic cylindrical beam of the length L and the radius R is considered, subject to the action of the arbitrary transverse loading $q(x)$ (see Fig. 1). The cylindrical beam is inhomogeneous, where the material properties are assumed to vary simultaneously along the length and radial directions. For such a structure, the Cartesian coordinates (x, y, z) and polar cylindrical coordinates (x, r, θ) are both used, where $y = r\cos\theta$, and $z = r\sin\theta$.

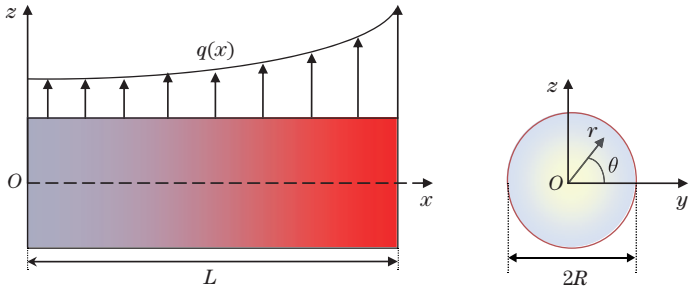

Fig. 1 Schematic diagram of a bi-directional FG cylindrical beam under the action of the transverse loading $q(x)$ with the corresponding coordinates (color online)

With the high-order cylindrical beam model[31], we can express the displacement field as

$$u_x = u_0(x,t) + z\varphi(x,t) - \frac{z^3 + zy^2}{3R^2}\Big(\frac{\partial w(x,t)}{\partial x} + \varphi(x,t)\Big), \tag{1}$$

$$u_y = 0, \tag{2}$$

$$u_z = w(x,t), \tag{3}$$

$$u_r = u_y\cos\theta + u_z\sin\theta = zw(x,t)/r, \tag{4}$$

where u_x, u_y, u_z, and u_r are the elastic displacement components in the x-, y-, z-, and r-directions, respectively. u_0 is the axial displacement of any point on the neutral axis. $\varphi(x,t)$ and $w(x,t)$ are, respectively, the cross-sectional rotation and transverse displacements of the beam. Based on the small deformation assumption, the relations between the strain and displacement components can be derived as

$$\varepsilon_{xx} = \frac{\partial u_x}{\partial x} = \frac{\partial u_0}{\partial x} + z\frac{\partial \varphi}{\partial x} - \frac{z^3 + zy^2}{3R^2}\Big(\frac{\partial^2 w}{\partial x^2} + \frac{\partial \varphi}{\partial x}\Big), \tag{5}$$

$$\gamma_{xy} = \frac{\partial u_x}{\partial y} + \frac{\partial u_y}{\partial x} = -\frac{2zy}{3R^2}\Big(\frac{\partial w}{\partial x} + \varphi\Big), \tag{6}$$

$$\gamma_{xz} = \frac{\partial u_x}{\partial z} + \frac{\partial u_z}{\partial x} = \frac{3R^2 - 3z^2 - y^2}{3R^2}\Big(\frac{\partial w}{\partial x} + \varphi\Big), \tag{7}$$

$$\begin{aligned}\gamma_{xr} &= \frac{\partial u_r}{\partial x} + \frac{\partial u_x}{\partial r}\\ &= \cos\theta\frac{\partial u_y}{\partial x} + \sin\theta\frac{\partial u_z}{\partial x} + \frac{\partial u_x}{\partial y}\frac{\partial y}{\partial r} + \frac{\partial u_x}{\partial z}\frac{\partial z}{\partial r}\\ &= \sin\theta\frac{\partial u_z}{\partial x} + \cos\theta\frac{\partial u_x}{\partial y} + \sin\theta\frac{\partial u_x}{\partial z}\\ &= \frac{z}{r}\frac{\partial w}{\partial x} - \frac{2zy^2}{3R^2r}\Big(\frac{\partial w}{\partial x} + \varphi\Big) + \frac{z}{r}\varphi - \frac{3z^3 + zy^2}{3R^2r}\Big(\frac{\partial w}{\partial x} + \varphi\Big)\\ &= \frac{z}{rR^2}(R^2 - z^2 - y^2)\Big(\frac{\partial w}{\partial x} + \varphi\Big),\end{aligned} \tag{8}$$

where ε and γ are the normal strain and the shear strain, respectively.

According to the Saint-Venant principle, we can ignore the effects of σ_{yy}, σ_{zz}, and τ_{yz} for a cylindrical beam[32]. As a result, the 3D constitutive equations change to

$$\sigma_{xx} = E(x,r)\varepsilon_{xx} = E(x,r)\Big(\frac{\partial u_0}{\partial x} + z\frac{\partial \varphi}{\partial x} - \frac{z^3 + zy^2}{3R^2}\Big(\frac{\partial^2 w}{\partial x^2} + \frac{\partial \varphi}{\partial x}\Big)\Big), \tag{9}$$

$$\tau_{xy} = G(x,r)\gamma_{xy} = -G(x,r)\frac{2zy}{3R^2}\Big(\frac{\partial w}{\partial x} + \varphi\Big), \tag{10}$$

$$\tau_{xz} = G(x,r)\gamma_{xz} = G(x,r)\frac{3R^2 - 3z^2 - y^2}{3R^2}\Big(\frac{\partial w}{\partial x} + \varphi\Big), \tag{11}$$

$$\tau_{xr} = G(x,r)\gamma_{xr} = \frac{zG(x,r)}{rR^2}(R^2 - z^2 - y^2)\Big(\frac{\partial w}{\partial x} + \varphi\Big), \tag{12}$$

where σ and τ are the normal stress and the shear stress, respectively. $E(x,r)$ and $G(x,r)$ are the Young's modulus and the shear modulus, respectively, which are 2D continuous functions dependent on both x and r. From Eq. (12), it can be easily found that the shear stress τ_{xr} is zero at the circumference $z^2 + y^2 = R^2$, which means that the shear-free surface condition is identically satisfied in this model.

In this thesis, we mainly consider the bending and vibration in the vertical plane, while neglect the horizontal motion in the Oxy-plane. As a result, the equilibrium equations for the plane problem change to

$$\frac{\partial \sigma_{xx}}{\partial x} + \frac{\partial \tau_{xy}}{\partial y} + \frac{\partial \tau_{xz}}{\partial z} = \rho(x,r)\frac{\partial^2 u_x}{\partial t^2}, \tag{13}$$

$$\frac{\partial \sigma_{xz}}{\partial x} + \frac{\partial \tau_{yz}}{\partial y} + \frac{\partial \sigma_{zz}}{\partial z} = \rho(x,r)\frac{\partial^2 u_z}{\partial t^2}, \tag{14}$$

where $\rho(x,r)$ is the radial and length-dependent mass density of the beam. Integrating both sides of Eq. (13) over the cross-sectional area A yields

$$\frac{\partial N}{\partial x} = \rho_0(x)\frac{\partial^2 u_0}{\partial t^2} + \rho_1(x)\frac{\partial^2 \varphi}{\partial t^2} - \rho_3(x)\Big(\frac{\partial^3 w}{\partial x \partial t^2} + \frac{\partial^2 \varphi}{\partial t^2}\Big), \tag{15}$$

where

$$N = \int_A \sigma_{xx}\mathrm{d}A = E_0(x)\frac{\partial u_0}{\partial x} + E_1(x)\frac{\partial \varphi}{\partial x} - E_3(x)\Big(\frac{\partial^2 w}{\partial x^2} + \frac{\partial \varphi}{\partial x}\Big) \tag{16}$$

is the axial normal force, and

$$\begin{cases} E_0(x) = \displaystyle\int_A E(x,r)\mathrm{d}A, \quad E_1(x) = \int_A E(x,r)z\mathrm{d}A = 0, \\ E_3(x) = \displaystyle\int_A E(x,r)\frac{z^3+zy^2}{3R^2}\mathrm{d}A = 0, \end{cases} \tag{17}$$

$$\begin{cases} \rho_0(x) = \displaystyle\int_A \rho(x,r)\mathrm{d}A, \quad \rho_1(x) = \int_A \rho(x,r)z\mathrm{d}A = 0, \\ \rho_3(x) = \displaystyle\int_A \rho(x,r)\frac{z^3+zy^2}{3R^2}\mathrm{d}A = 0. \end{cases} \tag{18}$$

It should be noted that the following integral results have been used to derive Eq. (15):

$$\int_A \frac{\partial \tau_{xy}}{\partial y}\mathrm{d}A = \int_{-R}^{R}\mathrm{d}z\int_{-\sqrt{R^2-z^2}}^{\sqrt{R^2-z^2}}\frac{\partial \tau_{xy}}{\partial y}\mathrm{d}y = \frac{4G(x,R)}{3R^2}\Big(\frac{\partial w}{\partial x}+\varphi\Big)\int_{-R}^{R} z\sqrt{R^2-z^2}\mathrm{d}z = 0, \tag{19}$$

$$\int_A \frac{\partial \tau_{xz}}{\partial z}\mathrm{d}A = \int_{-R}^{R}\mathrm{d}y\int_{-\sqrt{R^2-y^2}}^{\sqrt{R^2-y^2}}\frac{\partial \tau_{xz}}{\partial z}\mathrm{d}z = 0. \tag{20}$$

In the absence of the applied axial force N, Eqs. (15) and (16) change to

$$E_0(x)\frac{\partial u_0}{\partial x} = 0, \quad \rho_0(x)\frac{\partial^2 u_0}{\partial t^2} = 0. \tag{21}$$

Now, applying Eqs. (9)–(11) into Eq. (13), multiplying both sides of Eq. (13) by z, and integrating both sides over the cross-sectional area A yield

$$\frac{\partial}{\partial x}\Big(\widehat{E}_2(x)\frac{\partial \varphi}{\partial x} - E_4(x)\frac{\partial^2 w}{\partial x^2}\Big) - \widehat{G}_0(x)\Big(\frac{\partial w}{\partial x}+\varphi\Big) = \widehat{\rho}_2(x)\frac{\partial^2 \varphi}{\partial t^2} - \rho_4(x)\frac{\partial^3 w}{\partial x \partial t^2}, \tag{22}$$

where

$$\widehat{E}_2(x) = E_2(x) - E_4(x), \quad E_2(x) = \int_A E(x,r)z^2\mathrm{d}A, \quad E_4(x) = \int_A E(x,r)\frac{z^4+z^2y^2}{3R^2}\mathrm{d}A, \tag{23}$$

$$\widehat{G}_0(x) = G_0(x) - G_2(x), \quad G_0(x) = \int_A G(x,r)\mathrm{d}A, \quad G_2(x) = \int_A G(x,r)\frac{3z^2+y^2}{3R^2}\mathrm{d}A, \tag{24}$$

$$\widehat{\rho}_2(x) = \rho_2(x) - \rho_4(x), \quad \rho_2(x) = \int_A \rho(x,r)z^2\mathrm{d}A, \quad \rho_4(x) = \int_A \rho(x,r)\frac{z^4+z^2y^2}{3R^2}\mathrm{d}A. \tag{25}$$

In the process of deriving the above formulae, the following integral results are used:

$$\int_A z\frac{\partial \tau_{xy}}{\partial y}\mathrm{d}A = \int_{-R}^{R}\mathrm{d}z\int_{-\sqrt{R^2-z^2}}^{\sqrt{R^2-z^2}} z\frac{\partial \tau_{xy}}{\partial y}\mathrm{d}y = -\frac{\pi}{6}R^2G(x,R)\Big(\frac{\partial w}{\partial x}+\varphi\Big), \tag{26}$$

$$\int_A z\frac{\partial \tau_{xz}}{\partial z}\mathrm{d}A = \int_{-R}^{R}\mathrm{d}y\int_{-\sqrt{R^2-y^2}}^{\sqrt{R^2-y^2}} z\frac{\partial \tau_{xz}}{\partial z}\mathrm{d}z = \frac{\pi}{6}R^2G(x,R)\Big(\frac{\partial w}{\partial x}+\varphi\Big) - \int_A \tau_{xz}\mathrm{d}A. \tag{27}$$

Furthermore, integrating both sides of Eq. (14) over the cross-sectional area A yields

$$\frac{\partial}{\partial x}\Big(\widehat{G}_0(x)\Big(\frac{\partial w}{\partial x}+\varphi\Big)\Big) = \rho_0(x)\frac{\partial^2 w}{\partial t^2} - q(x). \tag{28}$$

Up to now, we finally get two coupled dynamic governing equations (22) and (28) for a 2D FG cylindrical beams in terms of the transverse deflection w and the rotation φ. The stress resultants of the shear force Q and the bending moment M are defined as

$$Q=\int_A \tau_{xz}\mathrm{d}A=\widehat{G}_0(x)\Big(\varphi+\frac{\partial w}{\partial x}\Big), \tag{29}$$

$$M=\int_A \sigma_{xx}z\mathrm{d}A=\widehat{E}_2(x)\frac{\partial\varphi}{\partial x}-E_4(x)\frac{\partial^2 w}{\partial x^2}. \tag{30}$$

In the Timoshenko beam theory, the formula of the shear force is $Q=\int_A \kappa\tau_{xz}\mathrm{d}A$, where κ is the shear correction factor. Because the shear stress is assumed to be uniform in this theory, we naturally have to introduce a coefficient κ to relax the traction-free surface condition.

3 Bending of 2D FG cylindrical beams

For the bending of 2D FG circular beams, by removing all time-dependent terms, the governing equations (22) and (28) can be simplified as

$$\frac{\mathrm{d}}{\mathrm{d}x}\Big(\widehat{E}_2(x)\frac{\mathrm{d}\varphi}{\mathrm{d}x}-E_4(x)\frac{\mathrm{d}^2 w}{\mathrm{d}x^2}\Big)=\widehat{G}_0(x)\Big(\frac{\mathrm{d}w}{\mathrm{d}x}+\varphi\Big), \tag{31}$$

$$\frac{\mathrm{d}}{\mathrm{d}x}\Big(\widehat{G}_0(x)\Big(\frac{\mathrm{d}w}{\mathrm{d}x}+\varphi\Big)\Big)=-q(x). \tag{32}$$

Integrating both sides of Eq. (32) with respect to x from 0 to x yields

$$\frac{\mathrm{d}w}{\mathrm{d}x}+\varphi=\frac{-\int_0^x q(s)\mathrm{d}s+A_1}{\widehat{G}_0(x)}. \tag{33}$$

Substituting Eq. (32) into Eq. (31) and then integrating both sides of Eq. (31) with respect to x from 0 to x yield

$$\widehat{E}_2(x)\frac{\mathrm{d}\varphi}{\mathrm{d}x}-E_4(x)\frac{\mathrm{d}^2 w}{\mathrm{d}x^2}=-\int_0^x (x-s)q(s)\mathrm{d}s+A_1x+A_2. \tag{34}$$

Derivating both sides of Eq. (33) yields

$$\frac{\mathrm{d}\varphi}{\mathrm{d}x}+\frac{\mathrm{d}^2 w}{\mathrm{d}x^2}=\Big(\frac{1}{\widehat{G}_0(x)}\Big)'\Big(-\int_0^x q(s)\mathrm{d}s+A_1\Big)-\frac{q(x)}{\widehat{G}_0(x)}. \tag{35}$$

Solving the above linear equations (34) and (35), we can easily get the solution of $\frac{\mathrm{d}^2 w}{\mathrm{d}x^2}$ as

$$\frac{\mathrm{d}^2 w}{\mathrm{d}x^2}=A_1U(x)-A_2\frac{1}{E_2(x)}+V(x), \tag{36}$$

where

$$\begin{cases} U(x)=\dfrac{1}{E_2(x)}\Big(\Big(\dfrac{1}{\widehat{G}_0(x)}\Big)'\widehat{E}_2(x)-x\Big), \\ V(x)=\dfrac{1}{E_2(x)}\Big(\displaystyle\int_0^x q(s)(x-s)\mathrm{d}s-\widehat{E}_2(x)\Big(\Big(\dfrac{1}{\widehat{G}_0(x)}\Big)'\int_0^x q(s)\mathrm{d}s+\dfrac{q(x)}{\widehat{G}_0(x)}\Big)\Big). \end{cases}$$

Then, integrating two times from $x=0$ to x on both sides of Eq. (36) yields

$$w=A_1\int_0^x (x-s)U(s)\mathrm{d}s-A_2\int_0^x \frac{x-s}{E_2(s)}\mathrm{d}s+A_3x+A_4+\int_0^x (x-s)V(s)\mathrm{d}s, \tag{37}$$

where A_i ($i = 1, 2, 3, 4$) are unknown integration constants in the general solution, which can be determined by means of the boundary conditions. Inserting Eq. (37) into Eq. (33) yields

$$\varphi = A_1\Big(\frac{1}{\widehat{G}_0(x)} - \int_0^x U(s)\mathrm{d}s\Big) + A_2\int_0^x \frac{1}{E_2(s)}\mathrm{d}s - A_3 - \frac{1}{\widehat{G}_0(x)}\int_0^x q(s)\mathrm{d}s - \int_0^x V(s)\mathrm{d}s. \quad (38)$$

In addition, applying the above expressions of w and φ into Eqs. (29) and (30) yields

$$Q = A_1 - \int_0^x q(s)\mathrm{d}s, \quad (39)$$

$$M = A_1 x + A_2 - \int_0^x q(s)(x-s)\mathrm{d}s. \quad (40)$$

Substituting Eqs. (37) and (38) into the normal stress σ_{xx} and the shear stresses τ_{xz} and τ_{xz} yields

$$\sigma_{xx} = zE(x,r)\Big(A_1\Big(\Big(\frac{1}{\widehat{G}_0(x)}\Big)' - U(x)\Big) + \frac{A_2}{E_2(x)} - \Big(\frac{1}{\widehat{G}_0(x)}\int_0^x q(s)\mathrm{d}s\Big)' - V(x) - \frac{z^2+y^2}{3R^2}\Big(\frac{1}{\widehat{G}_0(x)}\Big(A_1 - \int_0^x q(s)\mathrm{d}s\Big)\Big)'\Big), \quad (41)$$

$$\tau_{xy} = -\frac{G(x,r)}{\widehat{G}_0(x)}\frac{2zy}{3R^2}\Big(A_1 - \int_0^x q(s)\mathrm{d}s\Big), \quad (42)$$

$$\tau_{xz} = G(x,r)\gamma_{xz} = \frac{G(x,r)}{\widehat{G}_0(x)}\frac{3R^2 - 3z^2 - y^2}{3R^2}\Big(A_1 - \int_0^x q(s)\mathrm{d}s\Big). \quad (43)$$

It is obvious that the above physical quantities will be uniquely determined when the four constants A_j are obtained. For instance, we consider a simply 2D FG cylindrical beam, where the corresponding boundary conditions can be stated as

$$w = 0, \quad M = 0, \quad x = 0, L. \quad (44)$$

In view of $w = 0$ and $M = 0$ at $x = 0$ and L, from Eqs. (37) and (40), one can derive four linear equations for A_i as

$$A_4 = 0, \quad (45)$$

$$A_2 = 0, \quad (46)$$

$$A_1\int_0^L (L-s)U(s)\mathrm{d}s - A_2\int_0^L \frac{L-s}{E_2(s)}\mathrm{d}s + A_3 L + A_4 = \int_0^L (s-L)V(s)\mathrm{d}s, \quad (47)$$

$$A_1 L + A_2 = \int_0^L q(s)(L-s)\mathrm{d}s. \quad (48)$$

Therefore, $A_2 = A_4 = 0$, and A_1 and A_3 can be obtained by solving the linear equations of Eqs. (47) and (48) as

$$A_1 = \frac{1}{L}\int_0^L q(s)(L-s)\mathrm{d}s, \quad (49)$$

$$A_3 = -\frac{1}{L^2}\int_0^L q(s)(L-s)\mathrm{d}s\int_0^L (L-s)U(s)\mathrm{d}s + \frac{1}{L}\int_0^L (s-L)V(s)\mathrm{d}s. \quad (50)$$

For other boundary conditions, we can use the similar method to determine the four constants which are omitted here.

4 Free vibrations of 2D FG cylindrical beams

In this section, we will study the free vibrations of 2D FG cylindrical beams. To this end, applying $q=0$ into Eqs. (22) and (28) yields the governing equations as

$$\frac{\partial}{\partial x}\Big(\widehat{E}_2(x)\frac{\partial\varphi}{\partial x}-E_4(x)\frac{\partial^2 w}{\partial x^2}\Big)-\widehat{G}_0(x)\Big(\frac{\partial w}{\partial x}+\varphi\Big)=\widehat{\rho}_2(x)\frac{\partial^2\varphi}{\partial t^2}-\rho_4(x)\frac{\partial^3 w}{\partial x\partial t^2}, \tag{51}$$

$$\frac{\partial}{\partial x}\Big(\widehat{G}_0(x)\Big(\frac{\partial w}{\partial x}+\varphi\Big)\Big)=\rho_0(x)\frac{\partial^2 w}{\partial t^2}. \tag{52}$$

Since the governing equations (51) and (52) are two coupled higher-order differential equations, it is almost impossible to find the closed-form solutions of Eqs. (51) and (52) for different inhomogeneities. Therefore, it is much desired to find a numerical method for dealing with the free vibrations of such beams effectively. If we can transform two coupled governing differential equations (51) and (52) into a single governing equation, it is going to be easier for our subsequent analysis. For this purpose, the deflection w and the rotation φ are assumed to be

$$w=\frac{1}{\rho_0(x)}\frac{\partial F(x,t)}{\partial x}, \tag{53}$$

$$\varphi=\frac{1}{\widehat{G}_0(x)}\frac{\partial^2 F(x,t)}{\partial t^2}-\frac{\partial}{\partial x}\Big(\frac{1}{\rho_0(x)}\frac{\partial F(x,t)}{\partial x}\Big), \tag{54}$$

where $F(x,t)$ is a new auxiliary function. Apply Eqs. (53) and (54) into Eq. (52). Then, one can check that the two sides of the equation are equal. After putting Eqs. (53) and (54) into Eq. (51), we can immediately get a single fourth-order partial differential governing equation as

$$\sum_{i=1}^{4}B_i(x)\frac{\partial^i F}{\partial x^i}-\Big(\sum_{i=0}^{2}C_i(x)\frac{\partial^i}{\partial x^i}\Big)\frac{\partial^2 F}{\partial t^2}+D(x)\frac{\partial^4 F}{\partial t^4}=0, \tag{55}$$

where

$$\begin{cases}
B_1(x)=\Big(E_2(x)\Big(\dfrac{1}{\rho_0(x)}\Big)''\Big)', \quad B_2(x)=E_2(x)\Big(\dfrac{1}{\rho_0(x)}\Big)''+\Big(2E_2(x)\Big(\dfrac{1}{\rho_0(x)}\Big)'\Big)',\\
B_3(x)=2E_2(x)\Big(\dfrac{1}{\rho_0(x)}\Big)'+\Big(\dfrac{E_2(x)}{\rho_0(x)}\Big)', \quad B_4(x)=\dfrac{E_2(x)}{\rho_0(x)},\\
C_0(x)=\Big(\widehat{E}_2(x)\Big(\dfrac{1}{\widehat{G}_0(x)}\Big)'\Big)'-1, \quad C_2(x)=\dfrac{\widehat{E}_2(x)}{\widehat{G}_0(x)}+\dfrac{\rho_2(x)}{\rho_0(x)},\\
C_1(x)=\Big(\dfrac{\widehat{E}_2(x)}{\widehat{G}_0(x)}\Big)'+\widehat{E}_2(x)\Big(\dfrac{1}{\widehat{G}_0(x)}\Big)'+\rho_2(x)\Big(\dfrac{1}{\rho_0(x)}\Big)', \quad D(x)=\dfrac{\widehat{\rho}_2(x)}{\widehat{G}_0(x)}.
\end{cases}$$

The advantage of this treatment is that the physical quantities of interest can be expressed by the auxiliary function $F(x,t)$. For example, the deflection w and the rotation φ can be determined by means of Eqs. (53) and (54), respectively. Keeping Eqs. (29) and (30) in mind, the bending moment M and the shear force Q can be derived in terms of F as

$$M=\widehat{E}_2(x)\frac{\partial}{\partial x}\Big(\frac{1}{\widehat{G}_0(x)}\frac{\partial^2 F}{\partial t^2}\Big)-E_2(x)\frac{\partial^2}{\partial x^2}\Big(\frac{1}{\rho_0(x)}\frac{\partial F}{\partial x}\Big), \tag{56}$$

$$Q=\frac{\partial^2 F}{\partial t^2}. \tag{57}$$

In order to analyze the free vibrations of the 2D FG circular cylindrical beams, the auxiliary function F can be expressed as

$$F = f(x)\mathrm{e}^{\mathrm{i}\omega t}, \tag{58}$$

where ω is the circular frequency. Plugging Eq. (58) into Eq. (55) yields

$$\sum_{i=1}^{4} B_i(x)\frac{\mathrm{d}^i f}{\mathrm{d}x^i} + \omega^2 \sum_{i=1}^{4} C_i(x)\frac{\mathrm{d}^i f}{\mathrm{d}x^i} + \omega^4 D(x) f = 0. \tag{59}$$

The key of the problem lies in exactly calculating the natural frequencies w by solving the fourth-order differential equation (59) associated with the corresponding boundary conditions.

4.1 Solution of the resulting eigenproblem

We know that Chebyshev polynomials play an important role in numerical calculation applications. In the following, a simple approach called the Chebyshev polynomial expansion method will be proposed to determine the eigenvalues, which are related to the natural frequencies. The solution $f(x)$ of Eq. (59) can be expressed approximately in terms of the shifted Chebyshev polynomials with respect to the length coordinate as

$$f(x) = \sum_{i=0}^{N} a_i T_i(x), \quad 0 \leqslant x \leqslant L, \tag{60}$$

where a_i and N are unknown coefficients and the orthogonal polynomial order, respectively. $T_i(x)$ are the first kind of Chebyshev polynomials over the interval $[0, L]$, which are defined by the following recurrence relations:

$$T_0(x) = 1, \quad T_1(x) = \frac{2x}{L} - 1, \tag{61}$$

$$T_{i+1}(x) = 2\Big(\frac{2x}{L} - 1\Big)T_i(x) - T_{i-1}(x). \tag{62}$$

It should be noted that the Chebyshev polynomial expansion (60) must satisfy the governing equation (59) and the boundary conditions at the ends of the beam simultaneously. Now, putting the Chebyshev expansion (60) into the governing equation (59) for each case, we have

$$\sum_{i=0}^{N} \Big(\sum_{k=1}^{4} B_k(x) T_i^{(k)}(x) + \omega^2 \sum_{k=0}^{2} C_k(x) T_i^{(k)}(x) + \omega^4 D(x) T_i(x) \Big) a_i = 0, \tag{63}$$

where $T_i^{(k)}(x) = \frac{\mathrm{d}^k T_i}{\mathrm{d}x^k}$. Multiplying both sides of Eq. (63) by factors $T_j(x)$ $(j = 0, 1, 2, \cdots, N-4)$ and then integrating both sides from 0 to 1 with respect to x yield $N - 3$ linear equations of unknown coefficients a_i as

$$\sum_{i=0}^{N} (I_{ji} + \omega^2 J_{ji} + \omega^4 K_{ji}) a_i = 0, \quad j = 0, 1, 2, \cdots, N-4, \tag{64}$$

where

$$\begin{cases} I_{ji} = \displaystyle\int_0^L \Big(\sum_{k=1}^{4} B_k(x) T_i^{(k)}(x) T_j(x) \Big) \mathrm{d}x, \\ J_{ji} = \displaystyle\int_0^L \Big(\sum_{k=0}^{2} C_k(x) T_i^{(k)}(x) T_j(x) \Big) \mathrm{d}x, \\ K_{ji} = \displaystyle\int_0^L D(x) T_i(x) T_j(x) \mathrm{d}x. \end{cases}$$

Next, take clamped-clamped (CC) 2D FG circular cylindrical beams as an example. Substitute the expansion (60) to the clamped conditions $w = \varphi = 0$ at $x = 0$. Then, the other two linear equations of $a_0, a_1, \cdots, a_N$ will be obtained as

$$\sum_{i=0}^{N} a_i T_i'(0) = 0, \tag{65}$$

$$\sum_{i=0}^{N} a_i \Big(\frac{T_i''(x)}{\rho_0(x)} + \Big(\frac{1}{\rho_0(x)} \Big)' T_i'(x) + \frac{\omega^2 T_i(x)}{\widehat{G}_0(x)} \Big)_{x=0} = 0. \tag{66}$$

On the other hand, applying the clamped conditions at $x = L$ yields

$$\sum_{i=0}^{N} a_i T_i'(L) = 0, \tag{67}$$

$$\sum_{i=0}^{N} a_i \Big(\frac{T_i''(x)}{\rho_0(x)} + \Big(\frac{1}{\rho_0(x)} \Big)' T_i'(x) + \frac{\omega^2 T_i(x)}{\widehat{G}_0(x)} \Big)_{x=L} = 0. \tag{68}$$

From Eqs. (64)–(68), we can find that a series of of linear algebraic equations for unknown coefficients a_i have been derived, which forms a system as

$$(\boldsymbol{I} + \omega^2 \boldsymbol{J} + \omega^4 \boldsymbol{K})(a_1, a_2, a_3, \cdots, a_{N+1})^{\mathrm{T}} = 0. \tag{69}$$

To make sure that the resulting linear system has a non-zero solution, the determinant of the coefficient matrix of the system should be zero, i.e.,

$$\det(\boldsymbol{I} + \omega^2 \boldsymbol{J} + \omega^4 \boldsymbol{K}) = 0. \tag{70}$$

It is clear that the obtained equation (70) is actually a polynomial in the natural frequency ω. With the help of scientific software, we can easily obtain the multi-roots of its positive solutions, which correspond to different orders of natural frequencies. For other relevant familiar end conditions, such as simply-simply (SS), clamped-simply (CS), and clamped-free (CF), we can also apply the Chebyshev expansion (60) to the corresponding boundary conditions for getting the last four linear equations, and making the first $N - 3$ linear equations as the same form as Eq. (64), where the details are omitted here. This treatment could give rise to a great simplification on studying the free vibrations of 2D FG circular cylindrical beams with different end supports.

5 Results and discussion

5.1 Model validation and convergence studies

In order to verify the introduced cylindrical beam model, we first present some results applied to static and vibrational problems on homogeneous cylindrical beams. In general, however, it is rather difficult to get the exact bending elasticity solutions of the cylindrical beam for complex loads under different boundary conditions[32], which can be completely solved only for some certain special cases. For example, consider a homogeneous cantilevered circular beam subjected to a concentrated force P at the free end, where the boundary conditions are

$$x = 0: \ w = 0, \quad \varphi = 0, \tag{71}$$

$$x = L: \ M = 0, \quad Q = P. \tag{72}$$

In this case, one can use the Saint-Venant semi-inverse method to get the exact solutions[33–34]:

$$\sigma_{xx} = Pz(x-L)/I, \tag{73}$$

$$\tau_{xy} = -\frac{(2\nu+1)Pyz}{4(\nu+1)I}, \tag{74}$$

$$\tau_{xz} = \frac{(2\nu+3)P}{8(\nu+1)I}\Big(R^2 - z^2 - \frac{1-2\nu}{3+2\nu}y^2\Big), \tag{75}$$

where ν is Poisson's ratio. Other exact bending solutions, e.g., cylindrical beams under concentrated force under CC, SS, or CS supported boundary conditions and cylindrical beams under linearly distributed loadings, etc., have seldom been found in literatures so far. The introduced high-order cylindrical beam model is used to analyze the bending of cylindrical beams. It is actually a simple matter to derive the solutions for different complex loads and boundary conditions. Putting the boundary conditions in Eqs. (71) and (72) into Eqs. (37)–(40), the unknown A_j can be easily determined. Then, plugging them into Eqs. (41)–(43) yields the expressions of the normal stress and the shear stresses for a homogeneous cylindrical beam as

$$\sigma_{xx} = Pz(x-L)/I, \tag{76}$$

$$\tau_{xy} = -yzP/(4I), \tag{77}$$

$$\tau_{xz} = P(3R^2 - 3z^2 - y^2)/(8I). \tag{78}$$

It is easily found that the expression of the normal stress σ_{xx} in Eq. (76) is identical to the exact solution (73). In addition, the distributions are similar between two results of the shear stresses. If we do not take the effect of Poisson's ratio into account, the present solutions (77) and (78) are equivalent to the exact results. Moreover, it should be noted that the Timoshenko beam theory cannot give the distribution of the shear stress at the cross-section, but only presents the shear force resultant at the cross-section.

For examining the convergence and effectiveness of the Chebyshev polynomial expansion method, next, we will study the free vibration of a homogeneous cylindrical beam with a uniform circular cross-section. The convergence and verification studies are performed by using different numbers of terms in the Chebyshev polynomial expansion. By using the proposed method, we calculate the dimensionless natural frequencies $\Omega_n = \omega_n R\sqrt{\rho/G}$ for CF cylindrical beams with various aspect ratios and truncation orders N, where the results are noted in Table 1. For comparison, the 3D solutions calculated by the Ritz method[35] and the Chebyshev-Ritz method[36] are also listed in this table. It can be found that the presented approach has a fast convergence rate. With an increase in the aspect ratio L/R, there is good agreement between our numerical results and the 3D solutions.

We further use the introduced model to analyze the free vibrations of linearly tapered cylindrical beams, where the Young's modulus and the mass density of the beams keep constants, and the radius R of the circular cross-section is assumed to be

$$R(x) = R_0 + (R_L - R_0)\frac{x}{L}, \quad 0 \leqslant x \leqslant L, \tag{79}$$

where R_0 and R_L are the corresponding radii of the cross-section at the ends $x = 0$ and $x = L$, respectively. Based on the 3D theory of elasticity, Kang and Leissa used the Ritz method to investigate the free vibration frequencies and mode shapes of such tapered beams with a circular cross-section for isotropic materials[37]. For different ratio values of $L/(R_0+R_L)$, the first three dimensionless natural frequencies $\Omega_n = \omega_n L\sqrt{\rho/G}$ $(n = 1, 2, 3)$ are evaluated for free-free (FF) boundary conditions, which are displayed in Table 2. We set Poisson's ratio $\nu = 0.3$ and the aspect ratio $R_L/R_0 = 3$ in this example. Compared with the results derived previously by the

Euler-Bernoulli beam theory[37], it is obvious that our results agree well with the 3D solutions. This indicates that the suggested high-order model and numerical method can effectively handle the dynamic analysis of cylindrical beams.

Table 1 First three dimensionless natural frequencies $\omega_n R\sqrt{\rho/G}$ for the CF uniform cylindrical beams

L/R	Ω_n	Present result				3D solution	
		$N=6$	$N=8$	$N=10$	$N=12$	Ref. [35]	Ref. [36]
6	Ω_1	0.073 052	0.073 057	0.073 057	0.073 057	0.075 17	0.075 1
	Ω_2	0.360 907	0.348 172	0.348 118	0.348 118	0.364 3	0.364 0
	Ω_3	0.852 525	0.786 059	0.784 290	0.784 279	0.818 6	0.818 0
10	Ω_1	0.027 549	0.027 551 7	0.027 551 7	0.027 551 7	0.027 97	0.027 9
	Ω_2	0.159 434	0.152 053 7	0.152 018	0.152 017 8	0.156 2	0.156 0
	Ω_3	0.408 074	0.371 456 6	0.370 583	0.370 577 8	0.382 8	0.382 4
20	Ω_1	0.007 035	0.007 035	0.007 035	0.007 035	0.007 089	0.007 1
	Ω_2	0.044 953	0.042 516	0.042 503	0.042 503	0.043 00	0.042 9
	Ω_3	0.127 411	0.113 434	0.113 137	0.113 135	0.114 9	0.114 7
40	Ω_1	0.001 768	0.001 768	0.001 768	0.001 768	0.001 77	0.001 8
	Ω_2	0.011 642	0.010 981	0.010 977	0.010 977	0.011 05	0.011 0
	Ω_3	0.034 476	0.030 387	0.030 301	0.030 300	0.030 54	0.030 4

Table 2 First three dimensionless natural frequencies $\omega_n L\sqrt{\rho/G}$ for the FF tapered cylindrical beams

$L/(R_0+R_L)$	Present result				Other solution	
	$N=6$	$N=8$	$N=10$	$N=12$	3D[37]	Euler-Bernoulli beam[37]
5	1.763 809	1.712 408	1.712 599	1.712 597	1.716	1.892
	4.362 515	3.975 176	3.941 934	3.941 184	3.966	4.907
	14.514 850	7.634 360	6.612 236	6.606 935	6.680	9.388
10	0.949 532	0.920 175	0.920 245	0.920 244	0.920 8	0.945 8
	2.655 055	2.332 774	2.295 360	2.294 751	2.300	2.454
	–	4.784 441	4.169 972	4.168 268	4.187	4.694
20	0.484 851	0.469 571	0.469 599	0.469 599	0.469 7	0.472 9
	1.428 524	1.228 676	1.205 438	1.205 096	1.206	1.227
	–	2.603 828	2.271 740	2.270 282	2.273	2.347
40	0.243 751	0.236 029	0.236 043	0.236 042	0.236 1	0.236 5
	0.729 755	0.623 114	0.610 817	0.610 641	0.610 7	0.613 4
	–	1.334 832	1.164 524	1.163 620	1.164	1.174

5.2 Bending of bi-directional FG cylindrical beams

In this section, we will discuss the bending behavior of bi-directional FG cylindrical beams with a uniform circular cross-section. A typical model called power-law distribution is analyzed, where the material properties are assumed to be

$$E(x,r) = E_{\mathrm{m}} + (E_{\mathrm{c}} - E_{\mathrm{m}})\Big(\frac{x}{L}\Big)^{p_x}\Big(\frac{r}{R}\Big)^{p_r}, \tag{80}$$

$$G(x,r) = G_{\mathrm{m}} + (G_{\mathrm{c}} - G_{\mathrm{m}})\Big(\frac{x}{L}\Big)^{p_x}\Big(\frac{r}{R}\Big)^{p_r}, \tag{81}$$

$$\rho(x,r) = \rho_{\mathrm{m}} + (\rho_{\mathrm{c}} - \rho_{\mathrm{m}})\Big(\frac{x}{L}\Big)^{p_x}\Big(\frac{r}{R}\Big)^{p_r}, \tag{82}$$

where p_x and p_r are the gradient parameters indicating the variations of the volume fraction through the x- and r-axes, respectively. E_{m} (E_{c}) and G_{m} (G_{c}) are the Young's modulus and

the shear modulus of metal (ceramic), respectively. Aluminum and zirconia are chosen as the two materials, where the properties for aluminum are $E_{\mathrm{m}} = 70\,\mathrm{GPa}$, $\rho_{\mathrm{m}} = 2\,702\,\mathrm{kg/m^3}$, and $\nu_{\mathrm{m}} = 0.3$ while for zirconia are $E_{\mathrm{c}} = 200\,\mathrm{GPa}$, $\rho_{\mathrm{c}} = 5\,700\,\mathrm{kg/m^3}$, and $\nu_{\mathrm{c}} = 0.3$. Now, let us make some observations on Eqs. (80)–(82). Set $p_x = 0$, which means that the Young's modulus, the shear modulus, and the mass density of the beam depend only on r. In this case, the cylindrical beam becomes the radial-dependent FG beam. Keep $p_r = 0$, which means that the beam becomes the axially FG cylindrical beam. If $p_x = 0$ and $p_r = 0$, the beam becomes a homogeneous cylindrical beam with a uniform cross-section.

Subject to a uniformly transverse loading, i.e., $q(x) = q_0$, the dimensionless transverse deflections $W(x) = \frac{100E_{\mathrm{m}}R^3}{q_0L^3}\omega(x)$ of bi-directional FG cylindrical beams are calculated for various values of the material gradient indices (p_x, p_r). The maximum results of the transverse deflection $W(L/2)$ under the SS boundary condition are listed in Table 3. For further comparison, the results of the dimensionless deflection obtained by the Timoshenko beam theory are also listed in Table 3 with the shear correction factor $\kappa = 6/7$. We can find that the results calculated by these two beam models appear to have good consistency. It can also be observed that an increase in the power-law gradient parameter p_x or p_r implies a stiffness-hardening effect of the FG beam, which can control the dimensionless maximum transverse deflection to increase monotonically. The results of the dimensionless maximum transverse deflection with CC supported ends are tabulated in Table 4.

Table 3 Dimensionless maximum transverse deflections $\frac{100E_{\mathrm{m}}R^3}{q_0L^3}\omega(L/2)$ of the SS beams

L/R	p_r	$p_x = 0$		$p_x = 1$		$p_x = 2$		$p_x = 4$	
		Present	Timoshenko	Present	Timoshenko	Present	Timoshenko	Present	Timoshenko
5	0	3.746 109	3.746 109	5.851 228	5.851 228	7.357 589	7.357 589	8.939 436	8.939 436
	0.2	3.902 783	3.891 837	6.001 485	5.992 910	7.477 002	7.470 310	9.014 801	9.008 782
	0.5	4.124 677	4.098 198	6.208 478	6.188 752	7.640 244	7.624 745	9.116 485	9.102 567
	1	4.462 543	4.413 313	6.512 362	6.478 025	7.877 063	7.849 830	9.261 112	9.236 731
	2	5.037 681	4.955 365	7.003 859	6.951 396	8.252 274	8.210 050	9.482 908	9.445 311
	5	6.234 961	6.118 154	7.945 842	7.880 390	8.940 900	8.886 688	9.865 569	9.817 517
10	0	6.224 948	6.224 948	9.566 572	9.566 572	12.222 101	12.222 101	15.118 161	15.118 161
	0.2	6.442 289	6.436 815	9.786 867	9.782 580	12.399 658	12.396 311	15.219 045	15.216 035
	0.5	6.753 002	6.739 762	10.094 658	10.084 795	12.644 832	12.637 083	15.356 469	15.349 510
	1	7.233 448	7.208 832	10.555 475	10.538 307	13.005 614	12.991 998	15.554 744	15.542 553
	2	8.074 449	8.033 290	11.322 987	11.296 756	13.589 979	13.568 867	15.866 061	15.847 262
	5	9.929 139	9.870 736	12.867 114	12.834 388	14.705 051	14.677 945	16.427 713	16.403 687

Table 4 Dimensionless maximum transverse deflections $\frac{100E_{\mathrm{m}}R^3}{q_0L^3}\omega(L/2)$ of the CC beams

L/R	p_r	$p_x = 0$	$p_x = 1$	$p_x = 2$	$p_x = 3$	$p_x = 4$
5	0	1.666 485	2.626 416	2.989 635	3.208 668	3.362 295
	0.2	1.770 761	2.723 928	3.078 133	3.290 352	3.437 962
	0.5	1.916 847	2.855 735	3.196 643	3.399 034	3.538 229
	1	2.134 839	3.043 137	3.363 002	3.550 337	3.677 129
	2	2.490 384	3.328 532	3.611 701	3.773 986	3.881 177
	5	3.151 914	3.807 161	4.016 228	4.131 470	4.204 480
10	0	1.703 621	2.677 056	3.079 232	3.321 309	3.483 547
	0.2	1.896 556	2.856 601	3.239 520	3.467 190	3.617 896
	0.5	1.783 560	2.752 686	3.147 035	3.383 209	3.540 676
	1	2.067 854	3.008 199	3.373 038	3.587 548	3.728 035
	2	2.938 289	3.695 266	3.957 063	4.102 508	4.193 336
	5	2.356 314	3.249 742	3.582 331	3.774 203	3.897 744

The variations of the dimensionless deflection $\frac{100E_mR^3}{q_0L^3}\omega(x)$ with the dimensionless coordinate x/L are illustrated in Figs. 2 and 3 for CS and CF bi-directional FG cylindrical beams, respectively, in which $p_r = 1$ and $L/h = 10$. It is observed from Figs. 2 and 3 that the maximum values of the transverse deflections for CS and CF beams are not located in the middle positions of the beams because of the asymmetrical boundary conditions.

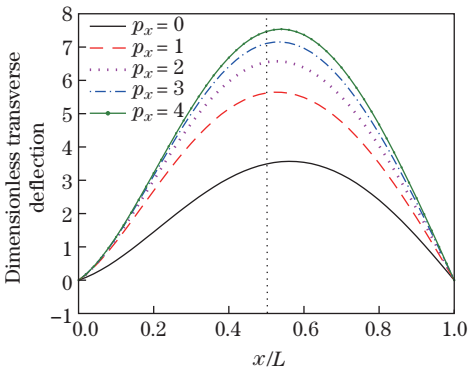

Fig. 2 Dimensionless transverse deflection $\frac{100E_mR^3}{q_0L^3}\omega(x)$ versus x/L for different p_x of CS bi-directional FG cylindrical beams (color online)

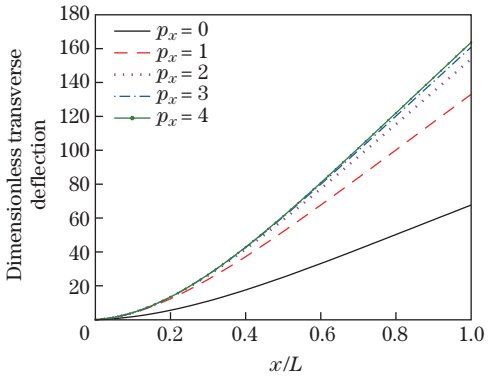

Fig. 3 Dimensionless transverse deflection $\frac{100E_mR^3}{q_0L^3}\omega(x)$ versus x/L for different p_x of CF bi-directional FG cylindrical beams (color online)

The effects of p_x on the dimensionless normal stress $\sigma_{xx}(\frac{L}{2}, 0, z)A/(q_0L)$ of a bi-directional FG cylindrical beam for SS supported ends are shown in Fig. 4, where $p_r = 1$ and $L/h = 10$. It can be found from Fig. 4 that when the gradient index p_x increases, the maximum normal stress decreases.

The variations of the dimensionless normal stress $\widetilde{\sigma}_{xx}(x, 0, -R)A/(q_0L)$ versus x/L are plotted in Fig. 5 under SS boundary conditions, where $p_r = 1$ and $L/h = 10$. It can be seen from Fig. 5 that when p_x increases, the normal stress decreases due to the fact that both the stiffness and the mass of the beam are increasing.

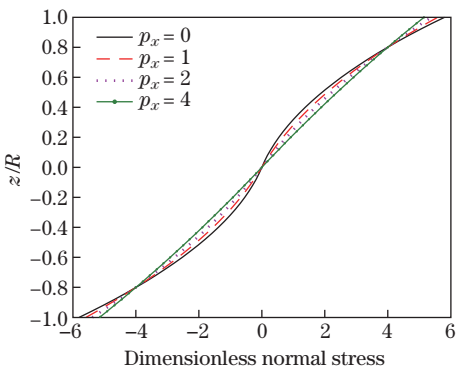

Fig. 4 Dimensionless normal stress $\sigma_{xx}(\frac{L}{2}, 0, z)A/(q_0L)$ versus z/R for different p_x of SS bi-directional FG cylindrical beams (color online)

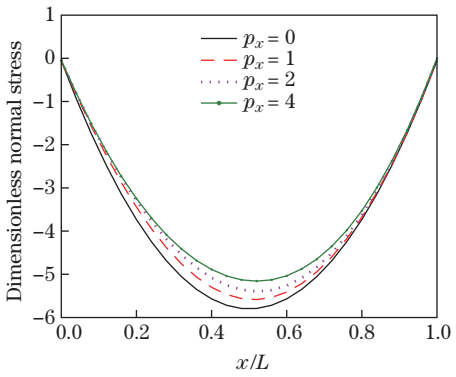

Fig. 5 Dimensionless normal stress $\widetilde{\sigma}_{xx}(x, 0, -R)A/(q_0L)$ versus x/L for different p_x of SS bi-directional FG cylindrical beams (color online)

The results of the normal stress distributions under CF boundary conditions have the same variation tendencies, as shown in Figs. 6 and 7, where $p_r = 1$ and $L/h = 10$. We derive the explicit expression of the shear stress under the SS and CF boundary conditions based on the high-order cylindrical beam model as

$$\text{SS}: \ \tau_{xy} = -\frac{q_0 G(x,r)}{\widehat{G}_0(x)} \frac{2zy}{3R^2}\Big(\frac{L}{2} - x\Big), \quad \tau_{xz} = \frac{G(x,r)}{\widehat{G}_0(x)} \frac{3R^2 - 3z^2 - y^2}{3R^2}\Big(\frac{L}{2} - x\Big); \tag{83}$$

$$\text{CF}: \ \tau_{xy} = -\frac{q_0 G(x,r)}{\widehat{G}_0(x)} \frac{2zy}{3R^2}(L - x), \quad \tau_{xz} = \frac{G(x,r)}{\widehat{G}_0(x)} \frac{3R^2 - 3z^2 - y^2}{3R^2}(L - x). \tag{84}$$

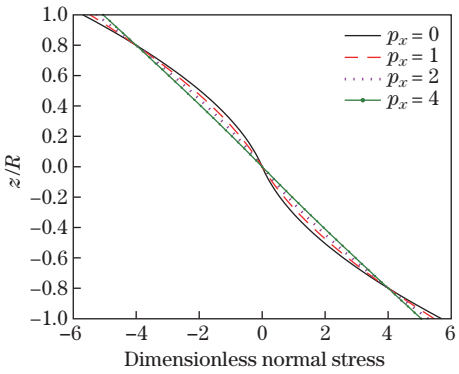

Fig. 6 Dimensionless normal stress $\sigma_{xx}(\frac{L}{2}, 0, z)A/(q_0 L)$ versus z/R for different p_x of CF bi-directional FG cylindrical beams (color online)

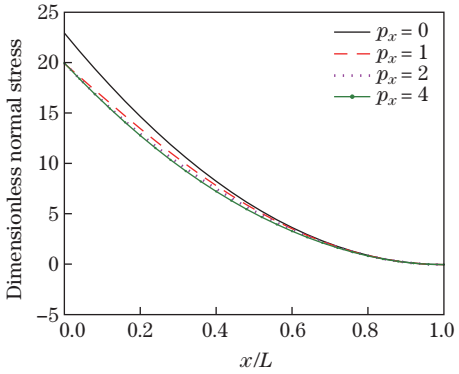

Fig. 7 Dimensionless normal stress $\widetilde{\sigma}_{xx}(x, 0, -R)A/(q_0 L)$ versus x/L for different p_x of CF bi-directional FG cylindrical beams (color online)

5.3 Natural frequencies of 2D FG cylindrical beams

Till now, the free vibrations of FG circular cylinders have seldom been discussed. Abadikhah and Folkow[29] adopted the Fourier and power series expansions to calculate the eigenfrequencies of simply supported cylinders by using the 3D elastodynamic theory for radially varying material inhomogeneities. Zhang et al.[30] proposed a higher-order shear deformation based spectral element model to calculate the natural frequency of FG cylindrical beams, where the material properties were assumed to vary along the r-axis. However, there has been no published work on discussing the dynamic behaviors of the axially or bi-directional FG cylindrical beam.

In order to investigate the effects of the power-law indeices p_x and p_r in Eqs. (80)–(82) on the natural frequency of 2D FG cylindrical beams, the results of the first three dimensionless natural frequencies $\Omega_n = \omega_n R\sqrt{\rho_{\mathrm{m}}/G_{\mathrm{m}}}$ under the SS and CF boundary conditions are presented with $N = 12$ in Tables 5 and 6, respectively. Some natural frequency results cited from Ref. [30] are also listed in Tables 5 and 6 with $p_x = 0$. Very good agreement between the present results and the existing numerical results[30] can be observed for the SS and CF 2D FG cylindrical beams. For a given value of the index p_r, one can find from Table 5 that the first three natural frequencies of the SS beam decrease with the increase in the gradient index p_x. When p_r increases, the first two dimensionless natural frequencies of the SS beam for a given value of the index p_x increase, reach the maximum values, and then decrease.

As the last example, we consider an exponential-law gradient model, where the material properties can be represented in an exponential form as

$$E(x,r) = E_{\mathrm{m}} \mathrm{e}^{\alpha_x \frac{x}{L} + \alpha_r \frac{r}{R}}, \quad G(x,r) = G_{\mathrm{m}} \mathrm{e}^{\alpha_x \frac{x}{L} + \alpha_r \frac{r}{R}}, \quad \rho(x,r) = \rho_{\mathrm{m}} \mathrm{e}^{\alpha_x \frac{x}{L} + \alpha_r \frac{r}{R}}, \tag{85}$$

Table 5 First three dimensionless natural frequencies $\Omega_n = \omega R\sqrt{\rho_{\rm m}/G_{\rm m}}$ of the SS beams, where $L/R = 10$

P_r	Ω_n	$p_x = 0$	$p_x = 0$[30]	$p_x = 1$	$p_x = 2$	$p_x = 3$	$p_x = 4$
0	Ω_1	0.088 381	–	0.083 340	0.080 376	0.078 828	0.077 959
	Ω_2	0.315 706	–	0.299 274	0.291 138	0.285 970	0.282 547
	Ω_3	0.618 955	–	0.586 233	0.570 437	0.561 246	0.555 330
0.2	Ω_1	0.089 012	0.088 9	0.083 722	0.080 622	0.078 985	0.078 059
	Ω_2	0.316 900	0.316 5	0.299 751	0.291 302	0.286 093	0.282 684
	Ω_3	0.619 356	0.618 6	0.585 963	0.570 031	0.560 905	0.555 065
0.5	Ω_1	0.089 661	–	0.084 092	0.080 853	0.079 127	0.078 147
	Ω_2	0.317 912	–	0.300 023	0.291 295	0.286 090	0.282 724
	Ω_3	0.618 996	–	0.585 102	0.569 183	0.560 226	0.554 531
1	Ω_1	0.090 214	0.090 1	0.084 362	0.081 009	0.079 214	0.078 193
	Ω_2	0.318 305	0.317 9	0.299 778	0.290 900	0.285 797	0.282 534
	Ω_3	0.616 985	0.616 2	0.583 074	0.567 495	0.558 906	0.553 485
2	Ω_1	0.090 295	–	0.084 275	0.080 923	0.079 136	0.078 119
	Ω_2	0.316 866	–	0.298 225	0.289 577	0.284 806	0.281 786
	Ω_3	0.611 194	–	0.578 565	0.564 059	0.556 249	0.551 362
5	Ω_1	0.088 461	0.088 3	0.082 941	0.080 060	0.078 548	0.077 696
	Ω_2	0.309 495	0.309 1	0.292 892	0.285 683	0.281 881	0.279 498
	Ω_3	0.595 376	0.594 7	0.567 856	0.556 338	0.550 313	0.546 579

Table 6 First three dimensionless natural frequencies $\Omega_n = \omega R\sqrt{\rho_{\rm m}/G_{\rm m}}$ of the CF beams, where $L/R = 10$

p_r	Ω_n	$p_x = 0$	$p_x = 0$[30]	$p_x = 1$	$p_x = 2$	$p_x = 3$	$p_x = 4$
0	Ω_1	0.032 064	–	0.022 980	0.021 939	0.022 035	0.022 351
	Ω_2	0.176 915	–	0.152 597	0.148 411	0.146 407	0.145 161
	Ω_3	0.431 271	–	0.394 514	0.385 845	0.378 624	0.373 073
0.2	Ω_1	0.032 310	0.032 2	0.023 358	0.022 325	0.022 409	0.022 708
	Ω_2	0.177 530	0.177 3	0.153 613	0.149 273	0.147 138	0.145 815
	Ω_3	0.431 453	0.430 9	0.395 384	0.386 364	0.379 101	0.373 608
0.5	Ω_1	0.032 565	–	0.023 831	0.022 815	0.022 883	0.023 160
	Ω_2	0.178 021	–	0.154 767	0.150 276	0.148 006	0.146 609
	Ω_3	0.431 077	–	0.396 147	0.386 804	0.379 561	0.374 182
1	Ω_1	0.032 789	0.032 7	0.024 440	0.023 458	0.023 505	0.023 750
	Ω_2	0.178 133	0.177 9	0.156 034	0.151 426	0.149 042	0.147 589
	Ω_3	0.429 512	0.429 0	0.396 535	0.386 994	0.379 904	0.374 747
2	Ω_1	0.032 842	–	0.025 243	0.024 336	0.024 357	0.024 555
	Ω_2	0.177 174	–	0.157 241	0.152 668	0.150 261	0.148 820
	Ω_3	0.425 251	–	0.395 825	0.386 464	0.379 844	0.375 141
5	Ω_1	0.032 181	0.032 1	0.026 317	0.025 605	0.025 594	0.025 718
	Ω_2	0.172 880	0.172 8	0.157 592	0.153 647	0.151 570	0.150 364
	Ω_3	0.413 922	0.413 5	0.391 615	0.383 680	0.378 412	0.374 782

where $E_{\rm m}$, $G_{\rm m}$, and $\rho_{\rm m}$ denote the Young's modulus, the shear modulus, and the mass density value at the reference point $(0, 0, 0)$, respectively. α_x and α_r are the gradation indices. To examine the effects of the material gradient indices α_x and α_r on the vibrational behaviors of 2D FG cylindrical beams, the first three dimensionless natural frequencies $\Omega_n = \omega_n R\sqrt{\rho_{\rm m}/G_{\rm m}}$ $(n = 1, 2, 3)$ are evaluated for SS and CC boundary conditions, where the results are tabulated in Tables 7 and 8, respectively. We set $\nu = 0.3$ and $L/h = 10$ in this example. It is obvious from Table 7 that if the exponential-law parameter α_x increases, the

Table 7 First three dimensionless natural frequencies Ω_n $(n = 1, 2, 3)$ of the SS beams with exponential-law distribution

α_r	Ω_n	$\alpha_x = 0$	$\alpha_x = 0.2$	$\alpha_x = 0.4$	$\alpha_x = 0.6$	$\alpha_x = 0.8$	$\alpha_x = 1$
0	Ω_1	0.075 943	0.075 908	0.075 803	0.075 629	0.075 386	0.075 074
	Ω_2	0.271 276	0.271 291	0.271 337	0.271 415	0.271 524	0.271 665
	Ω_3	0.531 849	0.531 868	0.531 927	0.532 026	0.532 164	0.532 342
0.2	Ω_1	0.076 825	0.076 789	0.076 683	0.076 506	0.076 258	0.075 941
	Ω_2	0.273 602	0.273 618	0.273 664	0.273 740	0.273 848	0.273 988
	Ω_3	0.534 915	0.534 935	0.534 993	0.535 091	0.535 227	0.535 404
0.4	Ω_1	0.077 673	0.077 637	0.077 529	0.077 349	0.077 098	0.076 775
	Ω_2	0.275 806	0.275 821	0.275 866	0.275 943	0.276 050	0.276 189
	Ω_3	0.537 755	0.537 774	0.537 832	0.537 928	0.538 064	0.538 238
0.6	Ω_1	0.078 488	0.078 452	0.078 342	0.078 159	0.077 904	0.077 577
	Ω_2	0.277 888	0.277 903	0.277 948	0.278 024	0.278 130	0.278 268
	Ω_3	0.540 376	0.540 395	0.540 453	0.540 548	0.540 682	0.540 855
0.8	Ω_1	0.079 270	0.079 233	0.079 122	0.078 937	0.078 678	0.078 346
	Ω_2	0.279 853	0.279 868	0.279 913	0.279 988	0.280 094	0.280 230
	Ω_3	0.542 790	0.542 809	0.542 865	0.542 960	0.543 092	0.543 263
1	Ω_1	0.080 020	0.079 982	0.079 869	0.079 681	0.079 419	0.079 082
	Ω_2	0.281 705	0.281 720	0.281 764	0.281 838	0.281 943	0.282 078
	Ω_3	0.545 006	0.545 024	0.545 080	0.545 174	0.545 305	0.545 474

Table 8 First three dimensionless natural frequencies Ω_n $(n = 1, 2, 3)$ of the CC beams with exponential-law distribution

α_r	Ω_n	$\alpha_x = 0$	$\alpha_x = 0.2$	$\alpha_x = 0.4$	$\alpha_x = 0.6$	$\alpha_x = 0.8$	$\alpha_x = 1$
0	Ω_1	0.148 090	0.148 121	0.148 214	0.148 369	0.148 588	0.148 871
	Ω_2	0.347 284	0.347 324	0.347 443	0.347 643	0.347 923	0.348 282
	Ω_3	0.590 518	0.590 556	0.590 671	0.590 862	0.591 130	0.591 475
0.2	Ω_1	0.149 094	0.149 125	0.149 219	0.149 375	0.149 595	0.149 880
	Ω_2	0.348 539	0.348 579	0.348 700	0.348 901	0.349 184	0.349 547
	Ω_3	0.591 713	0.591 752	0.591 868	0.592 060	0.592 330	0.592 678
0.4	Ω_1	0.150 026	0.150 057	0.150 151	0.150 308	0.150 529	0.150 816
	Ω_2	0.349 650	0.349 690	0.349 812	0.350 016	0.350 301	0.350 667
	Ω_3	0.592 714	0.592 753	0.592 870	0.593 064	0.593 336	0.593 686
0.6	Ω_1	0.150 888	0.150 919	0.151 013	0.151 171	0.151 394	0.151 681
	Ω_2	0.350 625	0.350 666	0.350 789	0.350 994	0.351 282	0.351 652
	Ω_3	0.593 536	0.593 575	0.593 692	0.593 888	0.594 162	0.594 514
0.8	Ω_1	0.151 682	0.151 714	0.151 809	0.151 967	0.152 191	0.152 480
	Ω_2	0.351 474	0.351 515	0.351 639	0.351 846	0.352 136	0.352 510
	Ω_3	0.594 192	0.594 232	0.594 350	0.594 547	0.594 822	0.595 177
1	Ω_1	0.152 413	0.152 445	0.152 540	0.152 699	0.152 924	0.153 214
	Ω_2	0.352 205	0.352 247	0.352 372	0.352 581	0.352 873	0.353 250
	Ω_3	0.594 698	0.594 737	0.594 856	0.595 054	0.595 331	0.595 688

natural frequencies decrease, but the increase in α_r can result in the increase in the natural frequencies for SS beams. For CC beams, the natural frequencies gradually increase when the index α_x or α_r increases.

6 Conclusions

Based on the high-order circular beam theory, where the shear deformation and rotary inertia are both considered without introducing the shear correction factor, the bending and free

vibrations of 2D FG cylindrical beams are discussed. For any radial/axial nonhomogeneity of material properties, the coupled governing differential equations of the deflection and rotation are derived. The analytic bending solutions are derived in a closed form for different boundary conditions. By expanding the auxiliary function into shifted Chebyshev polynomials, the characteristic polynomial equations in natural frequencies are obtained. Higher accuracy can be achieved through increasing the order of Chebyshev polynomials. By comparing with the exact 3D solutions, we present some static and vibrational results of homogeneous cylindrical beams to verify the introduced cylindrical beam model. The effects of gradient indices on the transverse deflections, the stresses, and the natural frequencies of 2D FG cylindrical beams are studied. Compared with the results calculated by the Timoshenko beam theory and other exiting numerical results, the accuracy and effectiveness of the introduced approach can be confirmed.

Acknowledgment The author would like to give thanks to the reviewers for their useful suggestions to improve the original manuscript.

References

[1] KADOLI, R., AKHTAR, K., and GANESAN, N. Static analysis of functionally graded beams using higher order shear deformation theory. *Applied Mathematical Modelling*, **32**, 2509–2525 (2008)

[2] SINA, S. A., NAVAZI, H. M., and HADDADPOUR, H. An analytical method for free vibration analysis of functionally graded beams. *Materials and Design*, **30**, 741–747 (2009)

[3] THAI, H. T. and VO, T. P. Bending and free vibration of functionally graded beams using various higher-order shear deformation beam theories. *International Journal of Mechanical Sciences*, **62**, 57–66 (2012)

[4] SU, H., BANERJEE, J. R., and CHEUNG, C. W. Dynamic stiffness formulation and free vibration analysis of functionally graded beams. *Composite Structures*, **106**, 854–862 (2013)

[5] PRADHAN, K. K. and CHAKRAVERTY, S. Free vibration of Euler and Timoshenko functionally graded beams by Rayleigh-Ritz method. *Composites Part B*: *Engineering*, **51**, 175–184 (2013)

[6] LI, X. F., KANG, Y. A., and WU, J. X. Exact frequency equations of free vibration of exponentially functionally graded beams. *Applied Acoustics*, **74**, 413–420 (2013)

[7] YANG, Q., ZHENG, B. L., ZHANG, K., and LI, J. Elastic solutions of a functionally graded cantilever beam with different modulus in tension and compression under bending loads. *Applied Mathematical Modelling*, **38**, 1403–1416 (2014)

[8] SU, H. and BANERJEE, J. R. Development of dynamic stiffness method for free vibration of functionally graded Timoshenko beams. *Composite Structures*, **147**, 107–116 (2015)

[9] LEE, J. W. and LEE, J. Y. Free vibration analysis of functionally graded Bernoulli-Euler beams using an exact transfer matrix expression. *International Journal of Mechanical Sciences*, **122**, 1–17 (2017)

[10] VIET, N. V., ZAKIA, W., and UMERA, R. Analytical model of functionally graded material/shape memory alloy composite cantilever beam under bending. *Composite Structures*, **203**, 764–776 (2018)

[11] SHAHBA, A., ATTARNEJAD, R., TAVANAIE MARVI, M., and HAJILAR, S. Free vibration and stability analysis of axially functionally graded tapered Timoshenko beams with classical and non-classical boundary conditions. *Composites Part B*: *Engineering*, **42**, 801–808 (2011)

[12] HUANG, Y., YANG, L. E., and LUO, Q. Z. Free vibration of axially functionally graded Timoshenko beams with nonuniform cross-section. *Composites Part B*: *Engineering*, **45**, 1493–1498 (2013)

[13] RAJASEKARAN, S. and TOCHAEI, E. N. Free vibration analysis of axially functionally graded tapered Timoshenko beams using differential transformation element method and differential quadrature element method of lowest-order. *Meccanica*, **49**, 995–1009 (2014)

[14] TANG, A. Y., WU, J. X., LI, X. F., and LEE, K. Y. Exact frequency equations of free vibration of exponentially non-uniform functionally graded Timoshenko beams. *International Journal of Mechanical Science*, **89**, 1–11 (2014)

[15] CAO, D. X., GAO, Y. H., YAO, M. H., and ZHANG, W. Free vibration of axially functionally graded beams using the asymptotic development method. *Engineering Structures*, **173**, 442–448 (2018)

[16] ZHANG, X. F., YE, Z., and ZHOU, Y. J. J. A Jacobi polynomial based approximation for free vibration analysis of axially functionally graded material beams. *Composite Structures*, **225**, 111070 (2019)

[17] NEMAT-ALLA, M. Reduction of thermal stresses by developing two-dimensional functionally graded materials. *International Journal of Solids and Structures*, **240**, 7339–7356 (2003)

[18] KARAMANLI, A. Bending behaviour of two directional functionally graded sandwich. *Composite Structures*, **174**, 70–86 (2017)

[19] ZHAO, L., ZHU, J., and WEN, X. D. Exact analysis of bi-directional functionally graded beams with arbitrary boundary conditions via the symplectic approach. *Structural Engineering and Mechanics*, **59**, 101–122 (2016)

[20] PYDAH, A. and SABALE, A. Static analysis of bi-directional functionally graded curved beams. *Composite Structures*, **160**, 867–876 (2017)

[21] ARMAGAN, K. Elastostatic analysis of two-directional functionally graded beams using various beam theories and symmetric smoothed particle hydrodynamics method. *Composite Structures*, **160**, 653–669 (2017)

[22] LI, J., GUAN, Y. J., WANG, G. C., and ZHAO, G. Q. Meshless modeling of bending behavior of bi-directional functionally graded beam structures. *Composites Part B*: *Engineering*, **155**, 104–111 (2018)

[23] SIMSEK, M. Bi-directional functionally graded materials (BDFGMs) for free and forced vibration of Timoshenko beams with various boundary conditions. *Composite Structures*, **133**, 968–978 (2015)

[24] DENG, H. and CHEN, W. Dynamic characteristics analysis of bi-directional functionally graded Timoshenko beams. *Composite Structures*, **141**, 253–263 (2016)

[25] HUYNH, T. A., LIEU, X. Q., and LEE, J. NURBS-based modeling of bidirectional functionally graded Timoshenko beams for free vibration problem. *Composite Structures*, **160**, 1178–1190 (2017)

[26] NGUYEN, D. K., NGUYEN, Q. H., TRAN, T. T., and BUI, V. T. Vibration of bi-dimensional functionally graded Timoshenko beams excited by a moving load. *Acta Mechanica*, **228**, 141–155 (2017)

[27] KARAMANLI, A. Free vibration analysis of two directional functionally graded beams using a third order shear deformation theory. *Composite Structures*, **189**, 127–136 (2018)

[28] LAL, R. and DANGI, C. Thermomechanical vibration of bi-directional functionally graded nonuniform timoshenko nanobeam using nonlocal elasticity theory. *Composites Part B*: *Engineering*, **172**, 724–742 (2019)

[29] ABADIKHAH, H. and FOLKOW, P. D. Dynamic equations for solid isotropic radially functionally graded circular cylinders. *Composite Structures*, **195**, 147–157 (2018)

[30] ZHANG, X. F., ZHENG, S. W., and ZHOU, Y. J. J. An effective approach for stochastic natural frequency analysis of circular beams with radially varying material inhomogeneities. *Materials Research Express*, **6**, 105701 (2019)

[31] HUANG, Y., WU, J. X., LI, X. F., and YANG, L. E. Higher-order theory for bending and vibration of beams with circular cross section. *Journal of Engineering Mathematics*, **80**, 91–104 (2013)

[32] LOVE, A. E. H. *A Treatise on the Mathematical Theory of Elasticity*, Dover, New York (1944)

[33] TIMOSHENKO, S. P. and GOODIER, J. N. *Theory of Elasticity*, McGraw Hills, Singapore (1970)

[34] ASARO, R. and LUBARDA, V. *Mechanics of Solids and Materials*, Cambridge University Press, New York (2006)

[35] LEISSA, A. W. and SO, J. Y. Comparisons of vibration frequencies for rods and beams from one-dimensional and three-dimensional analyses. *The Journal of the Acoustical Society of America*, **98**, 2122–2135 (1995)

[36] ZHOU, D., CHEUNG, Y. K., LO, S. H., and AU, F. T. K. 3D vibration analysis of solid and hollow circular cylinders via Chebyshev-Ritz method. *Computer Methods in Applied Mechanics and Engineering*, **192**, 1575–1589 (2003)

[37] KANG, J. H. and LEISSA, A. W. Three-dimensional vibration analysis of thick, tapered rods and beams with circular cross-section. *International Journal of Mechanical Science*, **46**, 929–944 (2004)